ChemComm

Accepted Manuscript

ROYAL SOCIETY OF CHEMISTRY

rsc.li/chemcomm

View Article Online
DOI: 10.1039/C7CC06270B

Journal Name

COMMUNICATION

Assembly of the active center of organophosphorus hydrolase in metal–organic frameworks via rational combination of functional ligands

Received 00th January 20xx,
Accepted 00th January 20xx

DOI: 10.1039/x0xx00000x

www.rsc.org/

Mengfan Xia,[†a] Caixia Zhuo,[†a] Xuejuan Ma,[a] Xiaohong Zhang,[a] Huaming Sun,[b] Quanguo Zhai,[*b] Yaodong Zhang[*a]

Different from popular mimics of bimetallic nuclear center bridged by a hydroxide, total coordination sphere of the active center of organophosphorus hydrolase was assembled in metal–organic frameworks by rational design and combined ligands, which resulted in efficient destruction of nerve agent stimulants without a base as co-catalyst.

Acute toxicity of organophosphorus nerve agents that contain phosphonate ester bonds is associated with their capability to bind to acetylcholinesterase. This bond causes neuromuscular paralysis and organ failure.[1] Recent abuse of nerve agents,[2] especially in military events in Syria and assassination in Malaysia, resulted in development of effective strategies for rapid detection and destruction of these chemical warfare agents (CWAs)[3] (Fig. 1a).

In nature, organophosphorus hydrolase (OPH, EC 3.1.8.1) decomposes phosphate ester bonds with high activity.[4] OPH active sites comprise a pair of Zn^{2+}, bridged by a hydroxo ligand, one Zn^{2+}(α) center with His55 (*Pseudomonas diminuta*, Protein Data Bank (PDB) code 1HZY[5]), His57 and Asp301, and another Zn^{2+}(β) with His201 and His230 (Fig. 1b ; ESI,[†] Fig. S1). A plausible catalytic cycle of OPH based on results in experimental and computational chemistry exhibits synergistic effects of bimetal nuclear center and amino acid residues.[6] However, high cost and fragile nature of enzymes hinder their industrial applications.[1,3] The structure of an enzyme–product complex reveals the critical role of terminal hydroxide nucleophiles in the mechanisms of bacterial OPH and other binuclear zinc enzymes.[7] Binding of paraoxon (organophosphate, a nerve agent stimulant) with OPH (1HZY) was docked using Autodock 4.2,8 and the lowest binding energy measured −4.49 kcal/mol (ESI,[†]Fig. S1b).

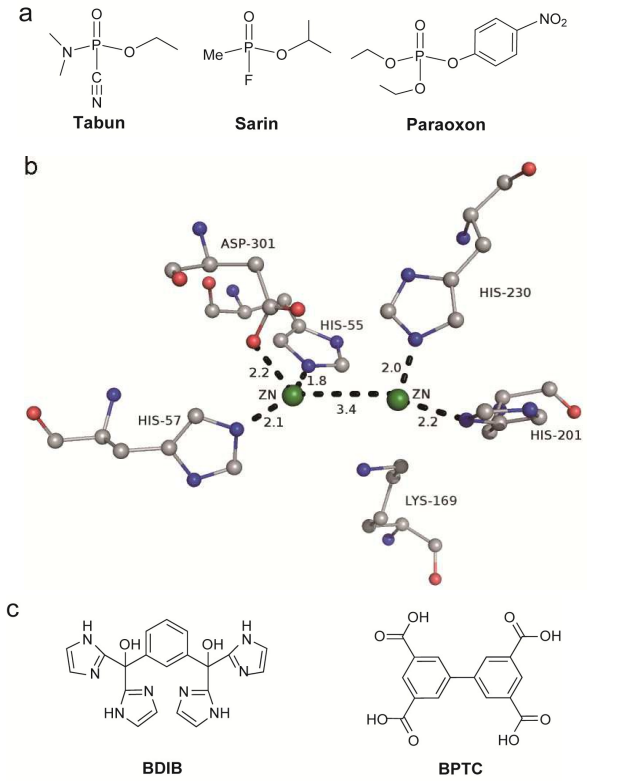

Fig.1 (a) Molecular structure of three organophosphates. (b) Coordination environment of bimetallic active site region for OPH. Extraction from structure of OPH (PDB code 1HZY) using Autodock 4.2. For clarity, bridged hydroxide and carboxylated lysine are not shown. (c) Structural formula of ligands of BDIB and BPTC.

A wide variety of enzymes mimic catalytically degraded CWAs, including many coordination complexes,[9] porous organic polymers,[10] metal oxides,[11] and metal–organic frameworks(MOFs).[12] Most of these artificial enzymes with high OPH-like activity originate from mimicry of bimetallic Zn^{2+} center. Structural motif of binuclear metal center was detected in the amidohydrolase superfamily of enzymes,

[a] *Key Laboratory of Analytical Chemistry for Life Science of Shaanxi Province, Key Laboratory of Applied Surface and Colloid Chemistry, Ministry of Education, School of Chemistry and Chemical Engineering Shaanxi Normal University Changan West Road 620, 710119, Xi'an, China E-mail: ydzhang@snnu.edu.cn; Fax: +86-29-81530727;Tel: +86-29-81530726*
[b] *Key Laboratory of Macromolecular Science of Shaanxi Province, Key Laboratory of Applied Surface and Colloid Chemistry, Ministry of Education E-mail: zhaiqg@snnu.edu.cn*
† These authors contributed equally to this work.
Electronic Supplementary Information (ESI) available.See DOI: 10.1039/x0xx00000x

View Article Online
DOI: 10.1039/C7CC06270B

which include urease, adenosine deaminase, atrazine chlorohydrolase, and dihydroorotase.[13] However, urease and OPH do not catalyze degradation of organophosphates and urea, respectively.[14] Synergistic effects of functional groups (i.e., His55, His57, His201, His230, Asp301, Lys169, and bimetallic Zn^{2+}) in the active center of OPH are essential for their high catalytic efficiency. Therefore, the presence of the electron-rich nucleophile, such as dialkylaminopyridine (DAAP), was required for the efficient hydrolysis of CWAs using artificial OPH, which mimicked the binuclear zinc center bridged by a hydroxide.[11b, 12d] The coordinative attachment with supernucleophilic DAAP, such as dimethylaminopyridine (DMAP), or addition of bases, such as N-methylmorpholine (NMM)[11b] and N-ethylmorpholine (NEM),[12a,12b,12e] as co-catalyst (Table 1) is necessary to enhance hydrolytic activity of these kinds of artificial enzymes to activate metal-bound water molecules by polarization,[11b] which is similar to the roles of histidines as general bases in OPH catalysis.[15] Thus, practical applications (i.e., gas filters, protective clothing, and suits) of these materials still confront many issues.[3]

In this study, we focused on systematic assembly of functional groups of OPH active sites in MOFs. 1,3-Bis(diimidazole-2-ylhydroxymethyl)benzene (BDIB) was designed, synthesized and characterized to model the imidazole group of histidine and construct the bimetallic center (Fig. 1c, see Supporting Information for synthesis and characterization details, ESI,† Scheme S1 and Fig. S2-S5). The carboxyl groups of biphenyl-3,3',5,5'-tetracarboxylic acid (BPTC) might mimic the function of carboxyl group in Asp. These two ligands were rationally combined and thus resulted in a novel MOF, $Zn(BDIB)_{0.5}(BPTC)_{0.5}\cdot 3DMF$ (SNNU-101, DMF = dimethylformamide), which exhibits a three-dimensional (3D) framework (Fig. 2a, and see Supporting Information for the structure of SNNU-101, ESI,† Fig. S6 and S7) with permanent porosity and realizes degradation of nerve agent stimulants (such as paraoxon) by a convenient and efficient pathway without using bases as co-reactants.

SNNU-101 was readily synthesized by solvothermal reaction of $ZnSO_4\cdot 7H_2O$, BDIB, BPTC, and DMF at 65 °C for 72 h (see Supporting Information). Single-crystal X-ray diffraction (XRD) analysis showed that SNNU-101 crystallizes in a monoclinic system called *C*2/*c* space group[17] (see Supporting Information for the detailed crystallographic data and the selected bond distances and angles, Table S1- S3). The asymmetric unit of SNNU-101 contains one Zn atom, half BDIB, half BPTC, and three DMF molecules. Each Zn center connects two BPTC and one BDIB, and each BPTC links four Zn centers (Fig. 2b).

Overall, zinc ions and BPTC can be regarded as 3- and 4-connected nodes, respectively. Subsequently, SNNU-101 displayed a (3,4)-connected 3D network with a $(6^2\cdot 8^2\cdot 10^2)(6^2\cdot 8)_2$ topology. 1D channels with dimensions of

Table 1 Comparison of phosphate ester degradation by OPH and several biomimetic catalysts.

Catalyst	Co-Catalyst[a]	Conditions[b]	Activity[c]	Ref.
SNNU-101	×	DENP, pH 9.0, 25 °C	Vmax=0.75 μM min^{-1}, Km = 2.5 mM, TOF= 0.058 s^{-1}	This work
Crystal 1	×	DENP, pH 9.0, 25 °C	Vmax=0.37 μM min^{-1}, Km = 3.1 mM, TOF= 0.014 s^{-1}	This work
OPH	×	DENP, pH 9.0, 25 °C	kcat= 2100 s^{-1}, kcat/Km=4×107 M^{-1} s^{-1}	16
MIL-101	DMAP[d]	DENP, pH 10.0, R.T.	$t_{1/2}$ = 5.0 h	12d
CeO_2 NPs	0.45 M NMM	DENP, pH 10.0, 45 °C	Vmax = 1.56 mM min^{-1}, Km = 15.78 mM	11b
UiO-66	0.45 M NEM	DMNP, pH 10.0, 60 °C	TOF = 1.5 s^{-1}, $t_{1/2}$ = 45 min	12a
NU-1000	0.45 M NEM	DMNP, pH 10.0, R.T.	$t_{1/2}$ = 15 min, TOF = 0.06 s^{-1}	12b
MOF-808	0.40 M NEM	DMNP, R.T.	$t_{1/2}$ = 0.5 min, TOF = 1.4 s^{-1}	12e

[a] N-methylmorpholine: NMM; N-ethylmorpholine: NEM. DMAP: dimethylaminopyridine; [b] DENP: diethyl 4-nitrophenylphosphate; DMNP: dimethyl 4-nitrophenylphosphate; CHES: 2-(cyclohexylamino)ethanesulfonic acid; R.T.: room temperature. [c] Various reports on degradation of phosphate ester using OPH mimics have been provided.[3] [d] Coordinatively attaching MIL-101 with DMAP ligand. However, optimal conditions of different catalysts differ. To date, various index, such as, kcat, $t_{1/2}$, TOF, and/or V_0, are used for evaluation of catalytical activity. Catalytic efficiency of synthesized OPH mimic was evaluated according to that of natural OPH.

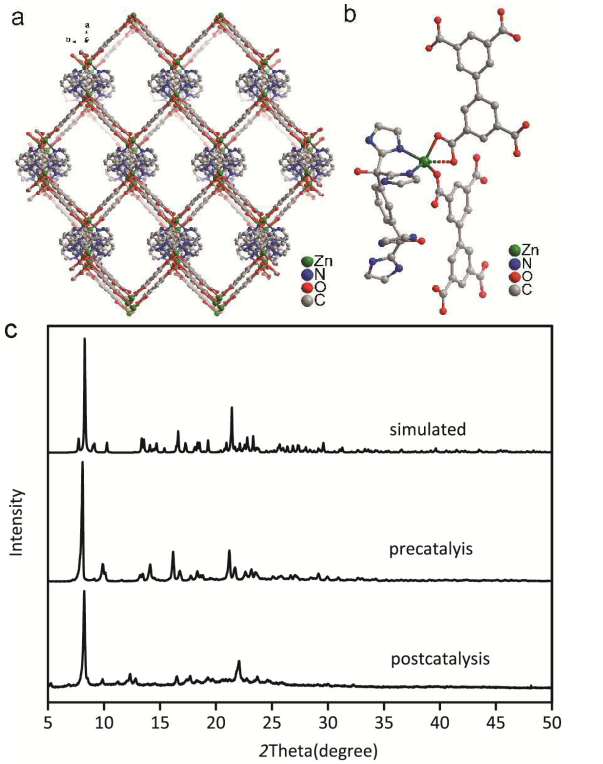

Fig.2 (a) 3D porous network of SNNU-101. (b) Coordination environment of Zn^{2+} in SNNU-101 (symmetry codes: #1 −x + 1, y, −z + 3/2). (c) PXRD data for SNNU-101 simulated pattern of precatalysis and in comparison with postcatalysis.

View Article Online
DOI: 10.1039/C7CC06270B

approximately 15 Å × 10 Å were observed along the c-axis directions. Purity and stability of SNNU-101 were confirmed using powder XRD (PXRD) (Fig. 2c). Thermal gravimetric analysis also demonstrated high thermal stability of SNNU-101 (ESI,† Fig. S8).

Given the risk in handling highly toxic CWAs, nerve agent stimulants are essential tools for evaluating phosphate ester decomposition.[3,12b,18] Catalytic efficacy of SNNU-101 for destruction of phosphate ester bonds was tested using a less toxic stimulant called paraoxon (diethyl 4-nitrophenylphosphate[12a,12b] (Fig. 3a). However, the catalytic efficacy may be different to that of the hydrolysis of other nerve agents. Degree of decomposition of paraoxon can be evaluated by measuring formation of *p*-nitrophenoxide at 400 nm at room temperature (Fig. 3b and 3c). No appreciable spontaneous hydrolysis of paraoxon was observed under identical reaction conditions without SNNU-101. Base conditions benefits substrate hydrolysis (ESI,† Fig. S9 and S10). Given the practical use, pH = 9.0 was selected to investigate catalytic efficiency. Steady-state kinetics of hydrolysis was investigated, whereas SNNU-101 (1.0 mg/mL) was dispersed in 20 mM 2-(cyclohexylamino) ethanesulfonic acid (CHES) buffer (pH = 9.0) without addition of base as co-reactants (detailed in Supporting Information). In this case, a typical Michaelis–Menten plot was obtained when concentration of paraoxon solution was increased from 1 mM to 7.5 mM (ESI,† Fig. S11). The straight line in the Lineweaver–Burk plot (Fig. 3d) suggests that SNNU-101 follows an enzyme-like kinetics. Maximum initial velocity (V_{max}) of the SNNU-101 (1.0 mg/mL)-catalyzed hydrolysis reaction of paraoxon measured 0.75 μM/min. Michaelis constant K_m reached 2.5 mM . Turnover frequency value (TOF) totaled 0.058 S^{-1}. The ordered channels or cavities in MOFs can offer the hydrophobic confined environment similar to natural enzymes and provide a highly density of substrate accessible active catalytic sites. This catalysis level surpassed efficiency of OPH mimics based on zinc(II) complex[19] or molecularly imprinted polymer.[20] Compared with several reported catalysts, such as UiO-66,[12a] NU-1000,[12b] and vacancy-engineered nanoceria (i.e., CeO_2 nanoparticles)[11b] (Table 1), SNNU-101 functions less efficiently. However, during activation, all these catalytic reactions require addition of general bases, such as NEM (0.45 M)[12a,12b] and NMM (0.45 M) ,[11b] which play the activation role similar to that of histidine in OPH.[15] Otherwise, catalytic efficiency becomes considerably lower. Addition of NMM (0.45 M) can also increase decomposition rate of paraoxon. However, enhanced catalytic efficiency of SNNU-101 was considerably lower than those of vacancy-engineered nanoceria[11b] and UiO-66[12a] because the imidazole groups of BDIB possibly play a similar role.

To illustrate the mechanism of catalysis, we synthesized another complex crystal (Crystal **1** = $Zn_2(SO_4)_2(BDIB)_2{\cdot}6H_2O$) that only uses BDIB as ligand. Crystal **1**[17] (see Supporting Information for the detailed crystallographic data and the selected bond distances and angles, ESI,† Fig. S12-S14, Table S4-S6) was synthesized using solvothermal reaction of $ZnSO_4{\cdot}7H_2O$, BDIB, and DMF at 80 °C for 48 h. The compound crystallizes in monoclinic crystal system with $P2_1/n$ space

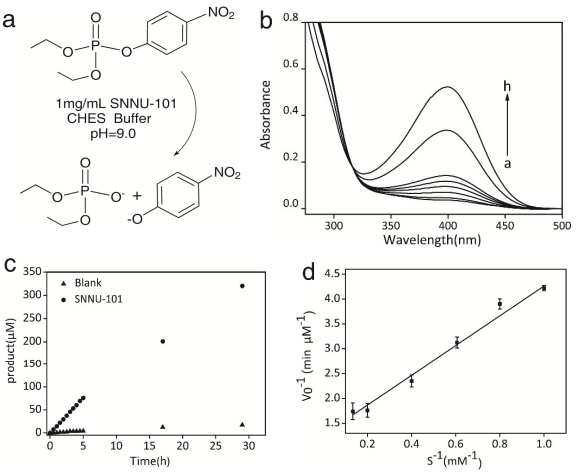

Fig.3 (a) Hydrolysis reaction of paraoxon catalyzed by SNNU-101. (b) UV–Vis spectra of the product p-nitrophenolate over time with SNNU-101. (c) Hydrolysis of paraoxon catalyzed by SNNU-101. (d) Lineweaver–Burk plot of kinetics data of paraoxon hydrolysis catalyzed by SNNU-101 (1.0 mg/mL SNNU-101 in 20 mM CHES, pH = 9.0 buffer solution at 25 °C; a–h= 0.5, 1, 2, 3, 4, 5, 17, and 29 h, respectively).

group with a highly symmetric structure. A binuclear metal center with two Zn(II) ions is bridged by two ligands. Each Zn(II) ion includes coordinatively unsaturated metal sites, rendering this binuclear Zn(II) complex a Lewis acid and allowing nucleophilic attack by certain nucleophiles.[12d, 21]

Notably, the zinc center in the SNNU-101 structure is coordinated with two imidazole groups of BDIB and two carboxyl groups of BPTC. In OPH, two Zn^{2+} ions are also coordinated with two imidazole groups of histidine residues and carboxyl groups of Asp or Lys, respectively. Interestingly, one carboxyl group of BPTC forms a pseudo-coordination bond (~2.30 Å) with Zn(II) ion in SNNU-101 (Fig. 4a). The side-chain carboxylate of Asp301 is within hydrogen-bonding distance from the bridging hydroxide in the active site and shuttle protons from the active site to bulk solvent during substrate turnover.[22] However, five zinc atoms in the structure of Crystal **1** are coordinated. In this structure, each zinc atom is coordinated with four imidazole groups and one sulfate ligand (Fig. 4b; ESI,† Fig. S12). Thus, coordination environment of Zn^{2+} in SNNU-101 is more similar to that in OPH. Catalytic activity of SNNU-101 is 47.6 times (initial rate) faster than that of Crystal **1** (Table 1 ; ESI,† Fig. S15 - S18). These results indicate that construction of coordination environment of two metal ions is highly important for catalytic efficiency on mimicry of OPH.

In the active center of natural OPH, two Zn^{2+} are bridged by

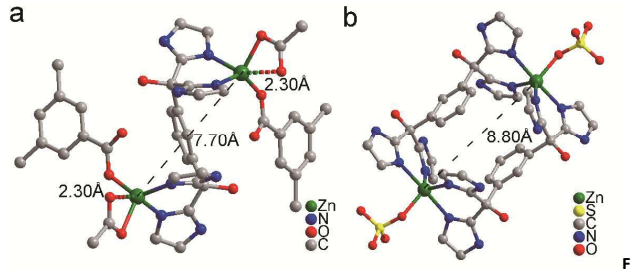

ig.4 Coordination environment and structure of Zn^{2+} in (a) SNNU-101 and (b) Crystal 1.

View Article Online
DOI: 10.1039/C7CC06270B

OH^- linkage, and bond length (or distance) for Znα…Znβ, Znα–OH^-, and Znβ–OH^- measures 3.40, 2.00, and ~1.99 Å, respectively.[5-6, 23].Distances of Zr…Zr in zirconium-based MOFs structures,[24] such as UiO-66,[12a] UiO-67,[25] MOF-808,[12e] and NU-1000[12b], total 3.53, 3.53, 3.56, and 3.53 Å, respectively, and are very close to the distance (3.40 Å) of Znα…Znβ in natural OPH. Interestingly, all these zirconium-based MOFs exhibit high catalytic activity. On the one hand, from the perspective of structure–activity relationship, Zr…Zr distance in the combined structure and hydrolysis mechanism of natural OPH favor synergistic catalysis. On the other hand, from the crystal structure analysis, although SNNU-101 effectively mimics coordination environment of Znα and Znβ in the active center of natural OPH through BDIB and BPTC, bimetallic Zn…Zn distance reached 7.70 Å (Fig. 4a) in SNNU-101 structure, and this condition is detrimental to the formation of hydroxyl bridge and synergistic effects of the two metal ions. Zn…Zn distance of Crystal **1** totaled 8.70 Å (Fig. 4b). As previously mentioned, this molecule performs a much lower activity levels than SNNU-101. When Zn…Zn distance in SNNU-101 structure is further optimized to mimic Znα…Znβ distance (3.40 Å) in the center of natural OPH, then the bridged hydroxo ligand may form more easily. Thus, biomimetic MOFs are expected to be synthesized with high catalytic activity.

In conclusion, SNNU-101 is an active biomimetic catalyst for paraoxon degradation without a base as co-catalyst (but increased degradation occurs at higher pH). SNNU-101 performance can be attributed to functionally mimic coordination environment and structure of binuclear metal center of natural OPH. The paper also demonstrated the importance of synergistic effects of functional groups on catalytic efficiency. A new ligand was designed to modulate Zn…Zn distance and to construct a bridged hydroxide in SNNU-101 to further develop destruction of CWAs.

This work was supported by the National Natural Science Foundation of China (21275097 and 21671126), Fundamental Research Fund for the Central Universities (GK201602010 and GK201701003) and the 111 Project(B14041) of China.

Notes and references

1 V.V. Singh, K. Kaufmann, d. Á. B. Esteban-Fernández, M. Uygun and J. Wang, *Chem. Commun.*, 2016, **52**, 3360.
2 M. Enserink, *Science*, 2013, **341**, 1050.
3 Y. J. Jang, K. Kim, O. G. Tsay, D. A. Atwood and D. G. Churchill, *Chem. Rev.*, 2015, **115**, PR1.
4 E. Ghanem and F. M. Raushel, *Toxicol. Appl. Pharmaco.l,* 2005, **207**, 459.
5 M. M. Benning, H. Shim, F. M. Raushel and H. M. Holden, *Biochemistry*, 2001, **40**, 2712.
6 P.-C. Tsai, Y. Fan, J. Kim, L. Yang, S. C. Almo, Y. Q. Gao and F. M. Raushel, *Biochemistry*, 2010, **49**, 7988.
7 (a) S.-L. Chen, W.-H. Fang and F. Himo, *J. Phys. Chem. B.*, 2007, **111**, 1253; (b) G. Parkin，*Chem. Commun*，2000, **32** ，1971; (c)G. Parkin，*Chem. Rev*. 2004, **104,** 699.
8 G. M. Morris, R. Huey, W. Lindstrom, M. F. Sanner, R. K. Belew, D. S. Goodsell and A. J. Olson, *J. Comput. Chem.*, 2009, **30**, 2785.
9 (a) O. Iranzo, A. Y. Kovalevsky, J. R. Morrow and J. P. Richard, *J. Am. Chem. Soc.*, 2003, **125**, 1988; (b) F. Carniato, C. Bisio, R. Psaro, L. Marchese and M. Guidotti, *Angew. Chem. Int. Ed.*, 2014, **53**, 10095; (c) S. A. Melnychuk, A. A. Neverov and R. S. B. Dr, *Angew. Chem. Int. Ed.*, 2006, **45**, 1767; (d) B. Kang, J. W. Kurutz, K.-T. Youm, R. K. Totten, J. T. Hupp and S. T. Nguyen, *Chem. Sci.*, 2012, **3**, 1938.
10 R. K. Totten, Y.-S. Kim, M. H. Weston, O. K. Farha, J. T. Hupp and S. T. Nguyen, *J. Am. Chem. Soc.*, 2013, **135**, 11720.
11 (a) K. Kim, O. G. Tsay, D. A. Atwood and D. G. Churchill, *Chem. Rev.*, 2011, **111**, 5345; (b) A. A. Vernekar, T. Das and G. Mugesh, *Angew. Chem. Int. Ed.*, 2016, **55**, 1412.
12 (a) M. J. Katz, J. E. Mondloch, R. K. Totten, J. K. Park, S. T. Nguyen, O. K. Farha and J. T. Hupp, *Angew. Chem. Int. Ed.*, 2014, **53**, 497; (b) J. E. Mondloch, M. J. Katz, W. C. Isley Iii, P. Ghosh, P. Liao, W. Bury, G. W. Wagner, M. G. Hall, J. B. DeCoste, G. W. Peterson, R. Q. Snurr, C. J. Cramer, J. T. Hupp and O. K. Farha, *Nat. Mater.*, 2015, **14**, 512; (c) P. Li, R. C. Klet, S. Y. Moon, T. C. Wang, P. Deria, A. W. Peters, B. M. Klahr, H. J. Park, S. S. Al-Juaid and J. T. Hupp, *Chemi. Commun.*, 2015, **51**, 10925; (d) S. Wang, L. Bromberg, H. Schreuder-Gibson and T. A. Hatton, *ACS Applied Materials & Interfaces*, 2013, **5**, 1269; (e) S.-Y. Moon, Y. Liu, J. T. Hupp and O. K. Farha, *Angew. Chem. Int. Ed.*, 2015, **54**, 6795.
13 L. Holm and C. Sander, *Proteins*, 1997, **28**, 72.
14 H. Shim and F. M. Raushel, *Biochemistry*, 2000, **39**, 7357.
15 G. Dodson and A. Wlodawer, *Trends Biochem. Sci.*, 1998, **23**, 347.
16 D. P. Dumas, S. R. Caldwell, J. R. Wild and F. M. Raushel, *J. Biol. Chem.*, 1989, **264**, 19659.
17 CCDC 1560464 (SNNU-101) and CCDC 1062340 ($Zn_2(SO_4)_2{\cdot}(BDIB)_2{\cdot}6H_2O$) contain the crystallographic data, which can be obtained free of charge from The Cambridge Crystallographic Data Centre.
18 Y. Liu, S.-Y. Moon, J. T. Hupp and O. K. Farha, *ACS. Nano.* , 2015, **9**, 12358.
19 A. Tamilselvi and G. Mugesh, *Chem.–Eur. J.*, 2010, **16**, 8878.
20 Z. Meng, T. Yamazaki and K. Sode, *Biotechnol. Lett.*, 2003, **25**, 1075.
21 (a) Y. K. Hwang, D. Y. Hong, J. S. Chang, S. H. Jhung, Y. K. Seo, J. Kim, A. Vimont, M. Daturi, C. Serre and G. Férey, *Angew. Chem. Int. Ed.*, 2008, **47**, 4144; (b) M. Banerjee, S. Das, M. Yoon, H. J. Choi, M. H. Hyun, S. M. Park, G. Seo and K. Kim, *J. Am. Chem. Soc.*, 2009, **131**, 7524.
22 S. D. Aubert, Y. Li and F. M. Raushel, *Biochemistry*, 2004, **43**, 5707.
23 C. J. Jackson, J.-L. Foo, N. Tokuriki, L. Afriat, P. D. Carr, H.-K. Kim, G. Schenk, D. S. Tawfik and D. L. Ollis, *Proc. Natl. Acad.Sci.*, 2009, **106**, 21631.
24 A. M. Plonka, Q. Wang, W. O. Gordon, A. Balboa, D. Troya, W. Guo, C. H. Sharp, S. D. Senanayake, J. R. Morris, C. L. Hill and A. I. Frenkel, *J. Am. Chem. Soc.*, 2017, **139**, 599.
25 S.-Y. Moon, G. W. Wagner, J. E. Mondloch, G. W. Peterson, J. B. DeCoste, J. T. Hupp and O. K. Farha, *Inorg. Chem.*, 2015, **54**, 10829.